Milling of submicron channels on gold layer using double charged arsenic ion beam

Ampere A. Tseng,[a] Ivan A. Insua, Jong S. Park, Bo Li, and George P. Vakanas
Department of Mechanical and Aerospace Engineering, and Center for Solid State Electronics Research, Arizona State University, Tempe, Arizona 85287-6106

(Received 26 June 2003; accepted 10 November 2003; published 14 January 2004)

The capability of using a focused ion beam (FIB) for milling of submicron channel structures on a gold layer is investigated. A double-charged arsenic (As^{2+}) FIB is adopted to assess the effect of the dwell time on the final profiles of the milled structures. A single-pass milling, which creates relatively shallow microchannels, is conducted in order to estimate the corresponding milling yields. The condition to provide a uniform ion flux in milling is first studied. The procedure on conducting the milling experiment is then presented. The atomic force microscope (AFM) is applied for measuring the profiles of the milled channels. Based on the AFM measurements, the milling yields have been estimated and compared with the sputtering yields predicted by a more sophisticated numerical simulation. The milling yield for the relatively shallow microchannels presently considered has been discovered to be roughly equal to the predicted normal-incidence sputtering yield. Consistence has also been found as the present findings have been compared with other channel milling studies, which had used different ion beams and target materials. FIB milling has been shown to be an effective tool for making submicron channels in gold layers. © *2004 American Vacuum Society.* [DOI: 10.1116/1.1640396]

I. INTRODUCTION

The focused ion beam (FIB) has been a valuable tool in the semiconductor industry for various applications, including mask repairing, device modification, failure analysis, and integrated circuit debugging. Because of the very short wavelength and very large energy density, the FIB has the ability for direct fabricating structures that have feature sizes at or below micrometers. Consequently, the FIB has recently become a popular selection in making various high-quality microdevices and high-precision components.

In this article, the capability of using FIB for milling submicron scale channel structures will be presented. Nano and microchannel structures have been widely used for many microelectromechanical systems devices, including microheat pipes, biosensors and detectors, thermal microreactors and microfluidic devices.[1,2] The channel structures are fundamental building blocks for these microcomponents or devices and are analogous to wires or thin film electrical interconnects in conventional integrated circuits. These devices and components have broad applications in aerospace, automotive, medical, pharmaceutical, instrument, electronic, and many other industries.

In the present research, the milled profiles on a gold film or layer will be specifically studied. The gold layer has been of considerable interest for electronic device fabrication. Not only does this layer provide excellent electrical connection among circuit elements, it can also be an integral part of the devices, such as in Schottky diodes and devices for interconnections without suffering from electromigration effects.[3] Because of its superior properties, the gold layer has also been used as etching masks for forming nanoscale GaAs columns,[4] in making superconductor devices,[5] and as absorbers on x-ray masks.[6,7] Recently, gold layers have become useful especially in fabrication of nanoscale structures. Self-assembled monolayers can be formed on a gold layer coated on a Si substrate using a photopatterning process.[8] Whitesides and Love[9] have developed a soft lithography technique to print a patterned organic molecule layer onto a gold coated Si substrate to form a self-assembled monolayer as a building block for three-dimensional (3D) nanostructures. The self-assembled monolayer pattern can be as thin as 50 nm. The gold coated Si substrate has also been used for nanomolding process. Ovchinnikov *et al.*[10] have used a process combining dry etching and annealing to convert a thin gold/chromium layer for making Si nanopillars. Consequently, the ability for patterning a gold layer is important for further advances in fabrication of both micro- and nano-devices.

In this article, a double-charged arsenic FIB will be used to mill submicron channels on a gold layer. The study will be specifically conducted by using single-pass (or scan) milling with different dwell times for making relatively shallow channels. The guidance for providing steady and uniform milling ion fluxes for making a smooth channel with continuously constant profiles will be studied. Channels will then be milled and the resulting profiles will be measured using the atomic force microscope (AFM). Based on these AFM measurement data, the effects of the dwell time on the final channel profile and the mean milling yield can be established. The numerical simulation using the Monte Carlo method will also be performed to predict the corresponding sputtering yield to compare and explain the milling yield presently estimated. Furthermore, comparison of the present findings with other nano- and microchannel milling experiments will be used to assess the effectiveness of the process applied for

[a]Author to whom correspondence should be addressed; electronic mail: ampere.tseng@asu.edu

 1071-1023/2004/22(1)/82/8/$19.00 ©2004 American Vacuum Society

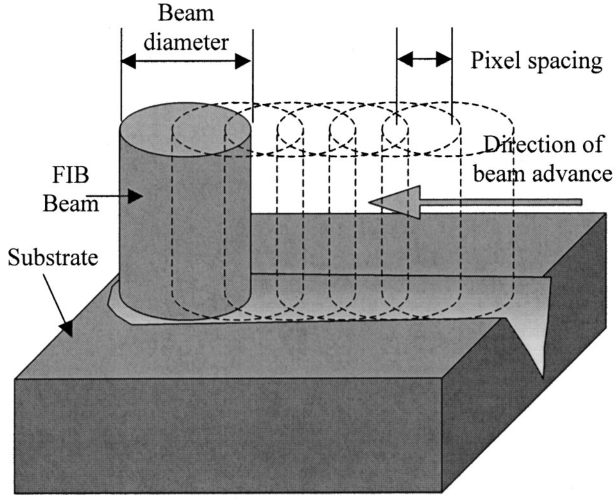

FIG. 1. Schematic of FIB milling.

milling submicrostructures. Finally, the concluding remarks are presented with suggestion for future work.

II. UNIFORM ION INTENSITY IN MILLING

In a modern computer-controlled FIB machine, milling is performed by a precise pixel-by-pixel movement. The process is also known as digital scan and is schematically shown in Fig. 1. To mill a submicron channel, the FIB follows a series of adjacent pixels representing the contour of the channel. The amount of time that the beam remains on a given target pixel is called the dwell time (t_d). The distance between the centers of two adjacent pixels is called the pixel spacing (p_s). To mill a channel with uniform cross sections, the ion intensity rate, or ion flux, with respect to the scan direction has to be unwavering or constant. To achieve this, the pixel spacing must be small enough to allow a proper overlap between adjacent pixels so that a smooth channel with a constant cross section can be milled. As a result, the threshold value for the minimum amount of the beam overlap should be known first and will be determined and discussed in this section.

A. Gaussion-shaped beam

Many investigators[11–13] indicated that the ion distribution of a FIB can be well described by a Gaussian distribution, which will be adopted in the present analysis and can be mathematically represented as[14]

$$D(r,\sigma)=\frac{D_0}{\sigma\sqrt{2\pi}}\exp\left(-\left(\frac{r}{\sigma\sqrt{2}}\right)^2\right), \tag{1}$$

where D is the Gaussian distribution; D_0 is the dose constant; r is the radial coordinate and the beam center is located at $r=0$; σ is the standard deviation of the Gaussian distribution, in which the beam full width at half maximum (FWHM) diameter (d_f) is equal to 2.355σ.[14] Here FWHM is commonly used for defining the beam diameter.

The total number of ions impinging on the target within one dwell time (t_d), is $I_p t_d/(nC_e)$, where I_p is the beam current and n is the number of charge, in which $n=1$ is for single-charged ion beams while $n=2$ is for double-charged ion beams. Here C_e is the charge of one electron or single-charged ion equal to 1.6×10^{-19} C. Consequently, the total beam input energy becomes $E_e I_p t_d/(nC_e)$, where E_e is the energy of one ion. Then, the constant D_0 can be obtained by satisfying the law of the conservation of energy in which the total input dose equals the total kinetic energy of the ions to the target within one dwell time, i.e.,

$$\int_0^{2\pi}\int_0^{\infty} D(r,\sigma)rdrd\theta=E_e I_p t_d/(nC_e). \tag{2}$$

Substituting Eq. (1) into the above equation, one can have

$$D_0=E_e I_p t_d/[nC_e(2\pi)^{1/2}\sigma]=0.94[E_e I_p t_d/(nC_e d_f)]. \tag{3}$$

If $D(r,\sigma)$ represents the ion density instead of the ion intensity, D_0 can be found as

$$D_0=0.94[I_p t_d/(nC_e d_f)]. \tag{4}$$

The energy of ion beams is usually measured in electron volts (eV), in which one eV is defined as the energy that an electron (or a single-charged ion) gains when moving through a potential difference of 1 V. Since the charge of one electron is 1.6×10^{-19} C, one eV is equal to 1.6×10^{-19} J. For a 90 keV FIB, double-charged ions need to be energized through a differential potential of 45 kV.

B. Uniform dose flux

During milling, since the beam moves in a pixel-by-pixel motion and stays at each pixel for a time equal to t_d, the superimposed or overlaid ion intensity (or density) over the target substrate can be conveniently expressed by the Cartesian coordinates (x,y) as

$$D(x,y,\sigma)=\frac{D_0}{\sigma\sqrt{2\pi}}\exp\left(-\left(\frac{y}{\sigma\sqrt{2}}\right)^2\right)\times\sum_{n=0}^{N}\exp\left(-\left(\frac{x-np_s}{\sigma\sqrt{2}}\right)^2\right), \tag{5}$$

where N is the total number of pixels involved in the process. During milling, the beam center starts at $x=0$ and $y=0$ and moves along the x direction.

Figure 2 shows the normalized ion flux or intensity at different normalized pixel spacing (p_s/σ), where the normalized ion intensity (or density) is defined as $\bar{D}=\sigma\sqrt{2\pi}D/D_0$. The Cartesian coordinates are also normalized by the standard deviation, σ. As shown in Fig. 2, at p_s/σ equal to 8, the ion flux of milling resembles each individual Gaussian distribution and no (or immeasurable) overlap is observed, while a small portion of overlap is observed at the tail regions when p_s/σ reduces to 4. As p_s/σ decreases to 2, the fluctuation of the ion flux becomes less than 3% of its mean. Finally, the fluctuation disappears as p_s/σ reaches 1.5 and the normalized ion flux becomes stable

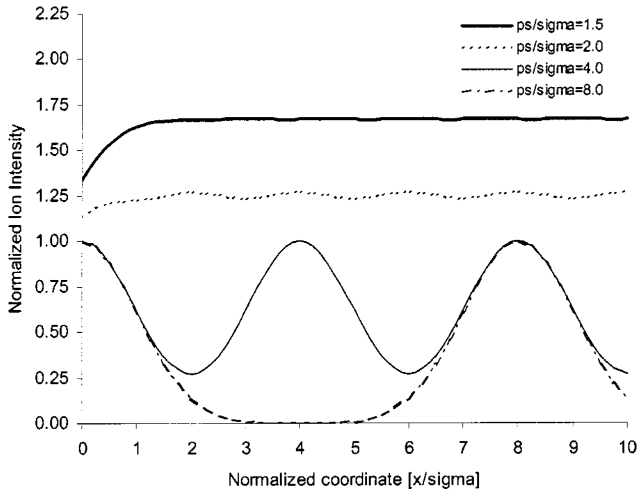

FIG. 2. Overlap effect on ion intensity distribution for Gaussian FIB milling.

and converges to a constant of 1.671, i.e., the fluctuation becomes immeasurable, less than 0.01%. The condition of $p_s/\sigma=1.5$ is equivalent to $p_s/d_f=0.637$ for a Gaussian distributed beam. To clearly illustrate the ion flux distribution, the 3D profiles for p_d/σ equal to 1.5 and 3.0 are shown in Figs. 3(a) and 3(b), respectively. This clearly indicates that to have a uniform scanning ion flux in channel milling, the normalized pixel spacing should be equal to or smaller than 1.5 (or $p_s/d_f=0.637$), while a fully drilling process for making an array of holes would require the normalized pixel spacing to be larger than 7 or 8. As a result, the drilling process can be considered as a special case of channel milling.

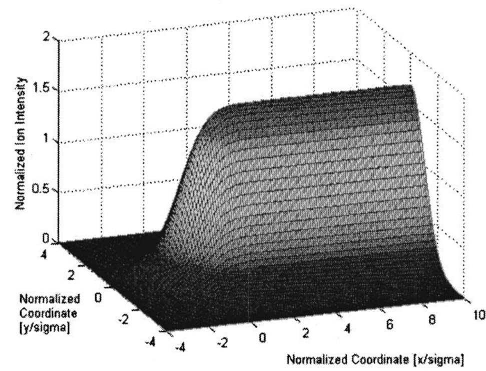

a) normalized pixel spacing equal to 1.5

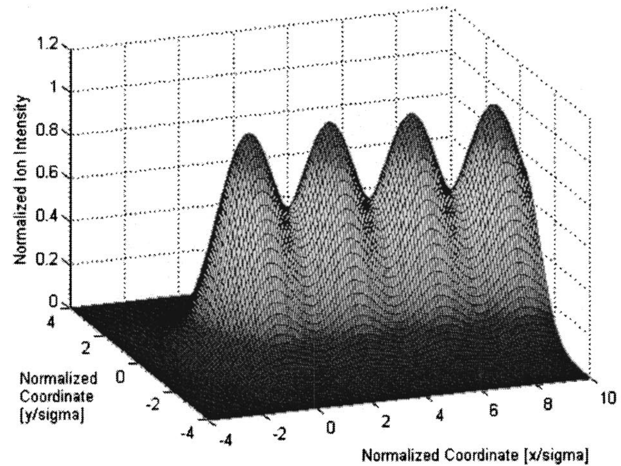

b) normalized pixel spacing equal to 3

FIG. 3. Three-dimensional normalized ion intensity distribution in FIB milling; (a) normalized pixel spacing equal to 1.5; (b) normalized pixel spacing equal to 3.0.

III. MILLING OF SUBMICRON CHANNELS

The FIB machine adopted is a two-lens system manufactured by Nano-FAB, Model 150, of Columbia, MD. The PdAsB alloy is used as the source to provide the double-charged arsenic ion beam for milling.

A. Sputtering yield prediction

Since the arsenic ion source is not often used for milling, reliable experimental data on its sputtering yield on gold targets are still not available. To provide a guidance for the milling experiment and a basis for examining the experimental results, a numerical analysis of the effects of ion energy on its sputtering yield is conducted. The software package TRIM (transport of ions in matter), is used. TRIM is a comprehensive Monte Carlo program that uses a Monte Carlo treatment of ion-atom collisions and has been widely used for predicting the sputtering yield for many different ions at a wide range of energy.[15,16]

Figure 4 shows the results of the TRIM simulations for the sputtering yield of an Au substrate by As ions at normal incidence as a function of the ion energy. For the sake of comparison, the Ga ion and Si substrate are also included in the simulation and shown in Fig. 4. While the Ga ion is the most popular ion species selected for FIB milling, Si is the most commonly used material in microdevices. Since TRIM is based on the Monte Carlo approach, the number of ions used in the simulation can have effects on the results. Normally, the TRIM predictions become converged when the ion number surpasses 500. To be conservative, 1000 ions are used for all of the TRIM simulations presented here.

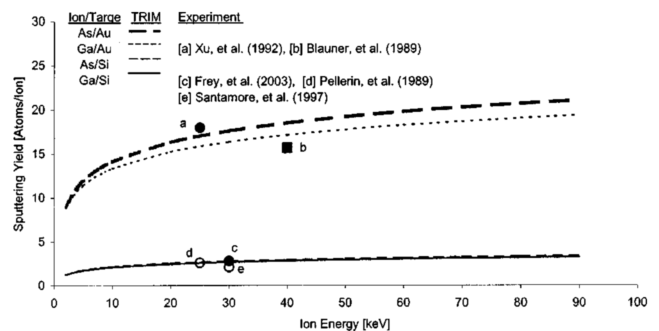

FIG. 4. Energy dependence of sputtering yields of Au and Si substrates by As and Ga ions.

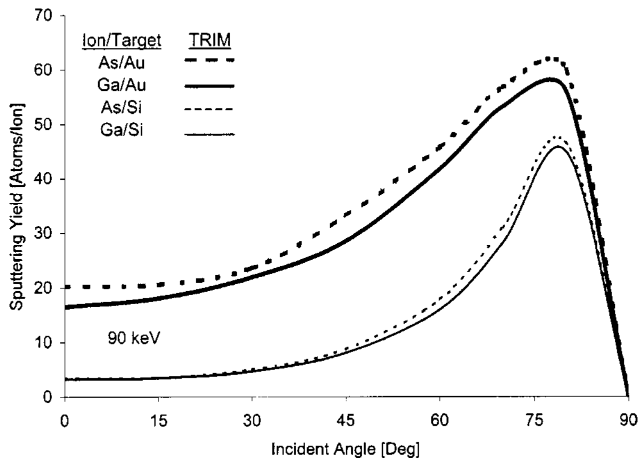

FIG. 5. Angular dependence of sputtering yields of 90 keV As and Ga ions on Au and Si targets.

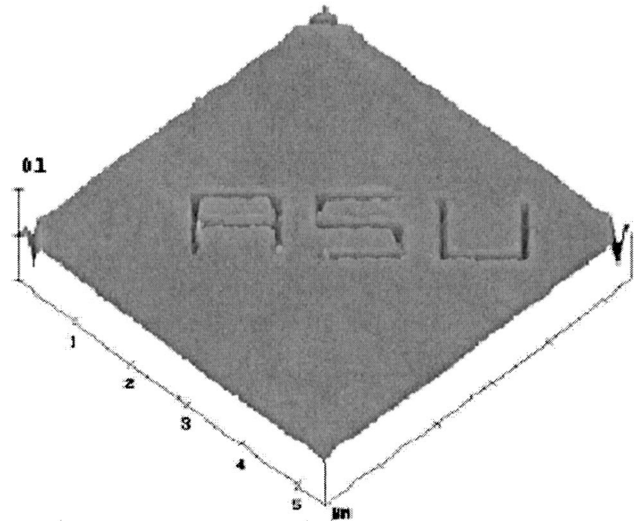

FIG. 6. AFM image of gold film coated at 25 °C with ASU pattern milled with 5 ms dwell time.

As shown in Fig. 4, the sputtering yield grows as the ion energy increases, but its rate of increase reduces as the ion energy increases. The figure also shows that the sputtering yield of the Au substrate is much higher than that of the Si substrate. Also, since the atomic weight of an $^{74.92}$As ion is slightly heavier than that of a $^{69.72}$Ga ion, the sputtering yield of As is accordingly higher than that of Ga. In general, the sputtering yield is dictated by the mass ratio of the bombarding ions to target atoms, and the larger the mass ratio, the higher the sputtering yield. Although the data are not shown, in most of the cases, the sputtering yield either levels off or decreases sometimes for ion energies higher than 100 keV, because implantation becomes the dominating factor in the interaction between the ions and the target at higher energies.[3] To gauge their reliability, the TRIM predictions are further compared to the experimental data reported by Blauner *et al.*,[17] Pellerin *et al.*,[18] Xu *et al.*,[19] Santamore *et al.*,[20] and Frey, Lehrer, and Ryssel.[21] As shown in Fig. 4, the TRIM predictions agree very well with these experimental data using Ga ions.

Figure 5 shows the TRIM simulation of the dependence of the sputtering yield on the incident angle at an ion energy of 90 keV in sputtering of Au and Si substrates. In simulation, the As and Ga ions considered are single charged and energized by a 90 kV electric potential. As shown in Fig. 5, for all cases considered, the increase in incidence angle raises the sputtering yield until it reaches its maximum near 80°; then it decreases very rapidly to zero as the incident angle approaches 90°. Figure 5 also shows that the sputtering yield of the Si substrate increases about ten times from the normal incidence to the angle at its peak while the corresponding sputtering yield for the Au substrate increases less than 2.5 times. The behavior of the angular dependence of sputtering yields has been observed by many researchers, including Santamore *et al.*[20] and Frey, Lehrer, and Ryssel.[21] Theoretically, since the energy intensity of a FIB generated using single-charged ions accelerated in a 90 kV differential potential is equivalent to that of double-charged ions accelerated in a 45 kV differential potential, the simulation results of Fig. 5 will be used for comparison with the experimental results using double-charged As ions accelerated in a 45 kV differential potential.

B. Gold layer preparation

The target material for the present study is a gold layer 125 nm thick while a silicon wafer serves as a substrate for the evaporation of the gold layer. The gold layer was coated or deposited by a high vacuum evaporation system with an ion-pumped glass bell jar capable of $\sim 6 \times 10^{-7}$ Torr. While the equilibrium melting temperature of gold is 1063 °C, the gold was melted at 1132 °C to attain a vapor pressure of 10^{-4} Torr suitable for deposition. System pressures were monitored by ion and thermal conductivity gauges while the layer thickness was measured by a quartz-crystal thickness monitor. The substrate stage is either water/liquid nitrogen cooled or resistance heated. A thermocouple in the stage indicates the substrate temperature.

Before FIB milling, the surface roughness of the gold films deposited at various speeds and substrate temperatures is first studied. At the substrate temperature of 25 °C, the typical arithmetic-mean surface roughness (R_a) is 1.0 nm and showed no significant change for the deposition speed increasing from 0.02 to 0.06 nm/s. However, for the substrate temperature elevating from 25 to 360 °C, R_a increases more than eightfold at a deposition rate of 0.02 nm/s. The AFM surface images for the samples at 25 and 360 °C are shown in Figs. 6 and 7, respectively. The image shown in Fig. 6 was taken after the sample was milled. The R_a for the sample shown in Fig. 7 is 8.9 nm, and it can cause inconsistent measurements in quantifying the dimensions of milled channels because the feature size of milled channels can be on the same order of magnitude with the roughness. Consequently, only the results based on the gold film coated at 25 °C are reported.

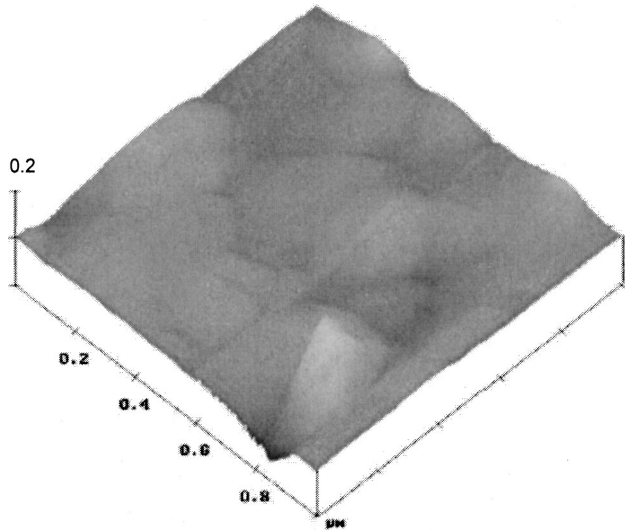

FIG. 7. AFM image of gold film coated at 360 °C with a typical surface roughness (R_a) of 8.9 nm.

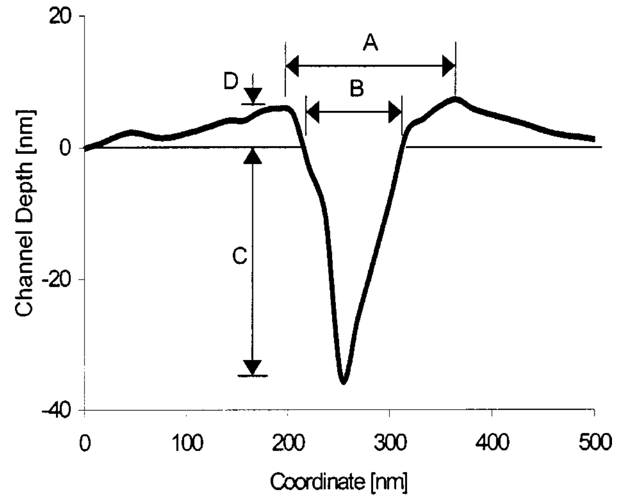

FIG. 9. AFM measurement and feature definition of typical channel cross section milled with 5 ms dwell time.

C. Milling experiments

As mentioned earlier, for ion energies higher than 100 keV, implantation becomes the dominant event and, thus, the sputtering yield either levels off or decreases sometimes. To have an effective ion performance, a 90 keV FIB with a beam current of 5 pA is selected in the present study. The double-charged As ions accelerated in a 45 kV differential potential are used to achieve the 90 keV beam energy. The pixel spacing (p_s) is set at 14.5 nm and the beam FWHM diameter (d_f) is set at 50 nm. The corresponding ratio of the pixel spacing to the beam diameter (p_s/d_f) is 0.29, which is smaller than 0.637, so that the scanning ion intensity or flux should be steady and uniform in the milling direction.

In the experiment, the dwell time is varied from 5 to 50 ms. Using raster scanning, a submicrochannel pattern as shown in Fig. 8 is milled by a single pass at each selected dwelling time. Each pattern consists of three sets of "ASU" with different sizes of characters. The largest character is 5 μm by 5 μm while the smallest character is 1 μm by 1 μm. The AFM image of an ASU pattern milled with a 5 ms dwell time has been shown in Fig. 6. The corresponding cross-sectional profile is shown in Fig. 9, and it possesses a V-shaped cross section with a maximum depth at the center and maximum width at the mouth. Ridges have been formed along the channel banks. Figure 9 also shows that the definition of the four features are used to characterize the profile of the V-shaped channel: A is the ridge width which is the distance between the ridge peaks, B is the mouth width which is the channel width with respect to the original surface, C is the depth from the original surface, and D is the ridge height.

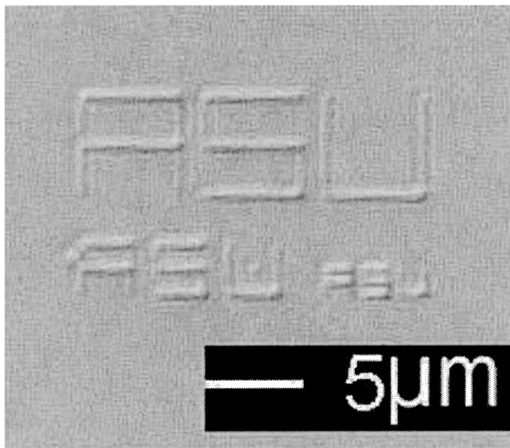

FIG. 8. Optical image of ASU patterns milled by 90 keV As^{++} FIB with 50 ms dwell time.

D. Profile measurements

Figure 10 shows the measurement results of the four profile features of the milled channel versus the dwell time (the amount of ion dose). The data for each dwell time shown in the figure are the mean of more than 100 measurements. The corresponding standard deviations are about 10% of its magnitude. To minimize the turning effects and to have consis-

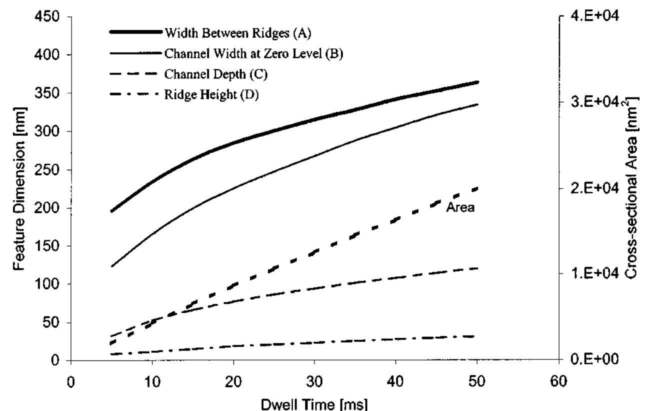

FIG. 10. Channel profile measurement for various dwell times.

tent results, each measurement is taken on a location (randomly selected) at least 300 nm away from any turning corners of the patterns. It is believed that the main reasons for causing the 10% standard deviations are due to the random nature of the redeposition in milling and the instability and the drift of the beam current.

As shown in Fig. 10, although all of the features increase with the dwell time, the increase rates are gradually reduced as the dwell time increases. This may indicate that a large amount of sputtered materials are redeposited into not only the ridge (outside the channel) but also inside the channel since the mouth width and the milling depth should increase proportionally with the dwell time without redeposition. Since only single pass is used, the channel is relatively shallow. The corresponding aspect ratio is of the order of 1/3 and is insensitive to the range of the dwell time considered. This may imply that it will be difficult to use a single-scan procedure to mill a high aspect-ratio channel because as the channel becomes deeper, more sputtered material is redeposited back into the channel and the wall becomes more tilted. Also, the measurements shown in Fig. 10 indicate that the mouth width is much larger than the FWHM diameter (d_f), by almost one order of magnitude. This may suggest that at higher dwell time, the ion intensity outside the FWHM core region is sufficiently high to produce sizable sputtering at a higher dwell time.

The increase of the ridge height shown in Fig. 10 can result from both the redeposited materials and the swelling of the substrate. Since the FIB resembles a Gaussian ion distribution, the intensity of the fringe (tail) of the beam is much smaller than its center core and is not strong enough to sputter materials but is sufficient for amorphization that induces substrate swelling. Normally, the intensity to cause swelling is 2–3 orders of magnitude lower than the sputtering intensity and the swelling disappears if the intensity increases, as reported by Frey, Lehrer, and Ryssel,[21] Stanishevsky,[22] and Lugstein *et al.*[23] During channel milling, the FIB always has a tail region that possesses the right dose to cause maximum swelling. Consequently, the swelling effect should be constant and not depend on the dwell time. Figure 10 clearly indicates that the ridge height and width increase with the dwell time. This may indicate that the ridge consists mainly of redeposited materials, which increase in volume with increasing dwell times or ion doses.

To establish the reliability of the measurements as those shown in Fig. 10, the profiles of the milled channels are examined by two types of scanning resolutions (*E* and *J* Scanners) and two types of tips (17 and 35°) when using the AFM. The resolution of the measurement using the *J*-type scanner is 15 nm compared to a resolution of 8 nm for the *E*-type scanner. Based on the measured data, it has been found that the measurement using the *E* scanner provides up to 5% higher values than those of the *J* scanner. Consequently, the *J* scanner is used for determining the channel locations while the *E* scanner is used to measure the channel profiles to obtain high-resolution results. During measurement, the scanning rate values are chosen low enough to minimize tip skipping for image capture purposes. Figure 11 shows the typical measurement results of the central depth of the milled channels using *E* scanning with both 17 and 35° tips. The figure shows that the measurement differences using the two different tips are insignificant. This may be due to the fact that the current milled channels are relatively shallow and their aspect ratio is relatively small and, thus, both tips can deliver consistent results. This confirms the validity of the present measurement results.

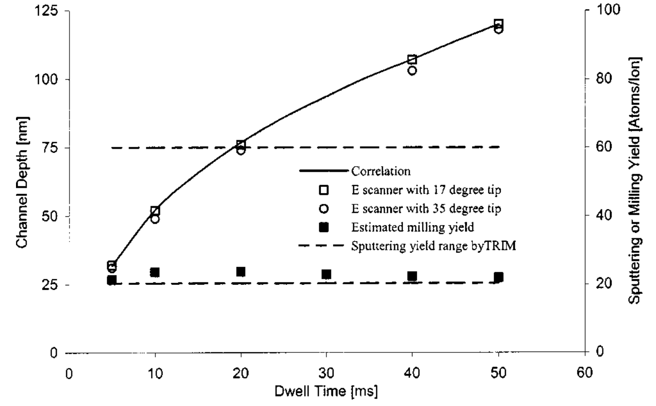

FIG. 11. Milling yield estimations with corresponding channel-depth measurements.

Furthermore, both Frey, Lehrer, and Ryssel[21] and Li *et al.*[24] have recently used 30 keV Ga^+ FIB to mill nanoscale channels with a single pass on Si substrates. They used different beam diameters at different beam currents and all learned that the channel profiles milled with a single pass are similar to that shown in Fig. 9, in a "V" shape. One of the channel profiles milled at 1 pA shown by Li *et al.*[24] is 10 nm deep while its mouth width is around 65 nm. Their results further confirm the present finding that the V-shaped channel profile is the inherent shape obtained by single-scan FIB milling.

E. Milling yield

If the channel cross section is V-shaped, the mean material removal rate (M) in a specific dwell time (t_d) can be approximated by

$$M = BCp_s/(2t_d), \tag{6}$$

where B and C are the data shown in Fig. 10. Since the As ions used are double charged ($n=2$) and the ion input rate to the target equals I_p, the corresponding milling rate per ion or the mean milling yield (m) can be expressed by

$$m = M/[\delta v I_p/(2C_e)], \tag{7}$$

where δv is the volume of one atom occupied in the substrate. Since the gold has a face-centered cubic (fcc) crystalline structure and each unit cell contains four atoms, one can find that $\delta v = b^3/4$, where b is the lattice parameter that is equal to 0.407 86 nm for gold.[25] Then, Eq. (7) can be expressed as $m = 4p_sC_eBC/(b^3 I_p t_d)$. In the formulation of Eq. (7), the effects of material point defects, such as vacancies, interstitial, and substitutional, are not considered. The com-

bined effects of point defects should be negligible because those defects most likely countervail each other.

Based on the data of B and C shown in Fig. 10, the mean milling yields can be calculated from Eq. (7) and are plotted in Fig. 11. As shown, the estimated milling yields vary from 21.4 atom/ion at 5 ms dwell time to 22.0 atom/ion at 50 ms dwell time with a maximum of 23.7 atom/ion near the dwell time of 20 ms. Two values of the sputtering yields predicted by TRIM for As ions to a gold target are also reported in Fig. 11 for comparison. These two values represent the minimum and the maximum sputtering yields obtained at incident angles of 0 and 80°, respectively. As shown, the calculated mean milling yields are almost independent of the dwell time and close to the value of the predicted sputtering yield at the normal incidence.

In FIB milling, material removals are mainly dictated by both sputtering and redeposition. It seems that, in the present channel milling, the decrease in milling yields due to redeposition almost counterbalances the increase due to the incident angle. This can also be observed by the fact that the cross-sectional area of the milled channel shown in Fig. 10 increases almost linearly with the dwell time or the amount of ion dose. The present finding of the mean milling yield being roughly equal to the sputtering yield at normal incidence is consistent with that recently reported by Lugstein *et al.*[23] Through a single-scan procedure, a 50 keV Ga FIB was used for milling channels on Si substrates, and the corresponding milling yield was found to be about 2.5 atoms/ion.[23] It can be observed from Fig. 4 that the minimum sputtering yield at the normal incidence predicted by TRIM is also approximately 2.5 atoms/ion.

The nonlinear relationship between the milled channel depth and the dwell time can be observed more clearly in Fig. 11. As shown, the rate of increase of channel depth gradually drops with the dwell time. Consequently, this observation does not imply that the milling rate drops as the dwell time increase because the mean milling yield is roughly invariant with respect to the dwell time.

IV. CONCLUDING REMARKS

FIB milling on a gold substrate has been successfully performed. The effects of the dwell time on the milled channel profile are specifically studied. The cross-sectional profiles are measured by atomic force microscopy and used to estimate the milling yield. The credibility of the measurement results is established by examining the data obtained by using different scanning modes with different shapes of AFM probes. The reliability of the estimated milling yields is verified by comparing the estimations with the sputtering yield obtained by numerical simulation.

The present research has developed simple and explicit criteria for obtaining a uniform ion intensity for channel milling that uses a pixel-by-pixel beam movement. A uniform input of ion intensity is the first step to mill a uniform channel with respect to the milling direction. The present results have indicated two observations: the channel is milled deeper as the dwell time is increased; and the rate of increase of the channel depth is gradually reduced with increasing dwell times. However, the reduction of the increase rate of the channel depth does not imply that the milling yield is also reduced. In fact, based on the profile measurements, the milling yields obtained are independent of the dwell time and match the values of the sputtering yield numerically predicted at the normal incidence. This may suggest that in the present channel milling, the effect of redeposition counterbalances the increase in milling yield due to increasing incident angles. It is to be noted that since the channels studied are milled by single-pass procedures and are relatively shallow, the present observation may not be directly applied to the situation involving multiple pass milling.

The present study has also indicated that FIB milling is an effective process to fabricate V-shaped submicron-scale channels. The study specifically indicates that a range of profiles of the channels can be obtained by controlling the ion energy and the amount of dose or the beam current. For example, the width of the channel mouth can be one order of magnitude larger than the beam diameter with a long dwell time. Because of this controllability, in addition to making channel structures, the FIB milling should have a great potential for fabricating other types of micron or submicron structures. In fact, the ability to make structures with micron or submicron sizes will be a key technology in the 21st Century and will have a revolutionary impact on every aspect of the manufacturing industry.[1,2,26] Tremendous challenges and opportunities await us to explore.

ACKNOWLEDGMENTS

The first author gratefully acknowledges the support of this study by the U.S. National Science Foundation under Grant Nos. DMI-0002466 and CMS-0115828. Special thanks go to Dr. David P. Pivin of Intel for his helpful discussions and for providing useful assistance for this study. The help from Bharath Leeladharan, Stefan Myhajlenko, and Martin Mitan of Arizona State University in conducting this research should be specifically acknowledged.

[1]A. A. Tseng, W. C. Tang, Y.-C. Lee, and J. Allen, J. Mater. Process. Manuf. Sci. **8**, 292 (2000).
[2]M. J. Madou, *Fundamentals of Microfabrication: The Science of Miniaturization*, 2nd ed. (CRC, Boca Raton, FL, 2002).
[3]S. K. Ghandhi, *VLSI Fabrication Principles: Silicon and Gallium Arsenide*, 2nd ed. (Wiley, New York, 1994).
[4]J. Ahopelto, V.-M. Airaksinen, E. Siren, and H. E.-M. Niemi, J. Vac. Sci. Technol. B **13**, 161 (1995).
[5]C.-H. Chen, I. Jin, S. P. Pai, Z. W. Dong, R. P. Sharma, C. J. Lobb, T. Venkatesan, K. Edinger, J. Orloff, J. Melngailis, Z. Zhang, and W. K. Chu, J. Vac. Sci. Technol. B **16**, 2898 (1998).
[6]M. L. Schattenburg, J. Carter, W. Chu, R. C. Fleming, R. A. Ghanbari, M. Mondol, N. Polce, and H. I. Smith, Mater. Res. Soc. Symp. Proc. **306**, 63 (1993).
[7]W. J. Dauksher, D. J. Resnick, W. A. Johnson, and A. W. Yanof, Microelectron. Eng. **23**, 235 (1994).
[8]J. Huang, D. A. Dahlgren, and J. C. Hemminger, Langmuir **10**, 626 (1994).
[9]G. M. Whitesides and J. C. Love, Sci. Am. **285(3)**, 39 (2001).
[10]V. Ovchinnikov, A. Malinin, S. Novikov, and C. Tuovinen, Mater. Sci. Eng., B **69**, 459 (2000).
[11]L. R. Harriott, J. Vac. Sci. Technol. A **8**, 899 (1990).

[12]G. Ben Assayag, C. Vieu, J. Gierak, P. Sudraud, and A. Corbin, J. Vac. Sci. Technol. B **11**, 2420 (1993).
[13]K. Edinger and T. Kraus, J. Vac. Sci. Technol. B **18**, 3190 (2000).
[14]E. W. Weisstein, MathWorld (CRC, Boca Raton, FL, 1999) (http://mathworld.wolfram.com/GaussianFunction.html).
[15]J. P. Biersack and L. G. Haggmark, Nucl. Instrum. Methods Phys. Res. B **174**, 257 (1980).
[16]J. W. Ward, J. Vac. Sci. Technol. B **3**, 207 (1985).
[17]P. G. Blauner, Y. Butt, J. S. Ro, and J. Melngailis, J. Vac. Sci. Technol. B **7**, 609 (1989).
[18]J. G. Pellerin, G. M. Shedd, D. P. Griffs, and P. E. Russell, J. Vac. Sci. Technol. B **7**, 1810 (1989).
[19]X. Xu, A. D. D. Ratta, J. Sosonkina, and J. Melngailis, J. Vac. Sci. Technol. B **10**, 2675 (1992).
[20]D. Santamore, K. Edinger, J. Orloff, and J. Melngailis, J. Vac. Sci. Technol. B **15**, 2346 (1997).
[21]L. Frey, C. Lehrer, and H. Ryssel, Appl. Phys. A: Mater. Sci. Process. **76**, 1017 (2003).
[22]A. Stanishevsky, Diamond Relat. Mater. **8**, 1246 (1999).
[23]A. Lugstein, B. Basnar, J. Smoliner, and E. Bertagnolli, Appl. Phys. A: Mater. Sci. Process. **76**, 545 (2003).
[24]H. W. Li, D. J. Kang, M. G. Blamire, and W. T. S. Huck, Nanotechnology **14**, 220 (2003).
[25]H. E. Boyer and T. L. Gall, *Metals Handbook*, Desk ed. (American Society for Metals, Metal Park, OH, 1985).
[26]M. C. Roco and W. S. Bainbridge, *Societal Implications of Nanoscience and Nanotechnology* (Kluwer, Hingham, MA, 2001).